Flow Marks in Injection Molding of Polypropylene and Ethylene–Propylene Elastomer Blends: Analysis of Morphology and Rheology

Bhaskar Patham,[1] Paul Papworth,[1] Krishnamurthy Jayaraman,[1] Chichang Shu,[2] Michael D. Wolkowicz[2]

[1]*Department of Chemical Engineering & Materials Science, Michigan State University, East Lansing, Michigan 48824*
[2]*Basell Polyolefins USA, Elkton, Maryland 21921*

Received 19 August 2004; accepted 29 September 2004
DOI 10.1002/app.21459
Published online in Wiley InterScience (www.interscience.wiley.com).

ABSTRACT: This paper reports an investigation of asynchronous flow marks on the surface of injection molded parts and short shots made from two different blends of polypropylene and ethylene–propylene random copolymer elastomers. Flow marks were observed on the surface with both blends; the spatial frequency of flow marks on the surface was greater in the blend B1, which also exhibited a greater contrast between the surface regions. The same blend was distinctly faster in the linear viscoelastic tests of shear creep recovery and shear viscosity growth. The degree of contrast between the flow-mark regions and the out-of-flow-mark regions was examined with a detailed analysis of SEM micrographs of the surface regions as well as the near wall regions from short shots. This revealed that the dispersed phase was highly stretched to cylindrical strands in the glossy surface regions of both blends and retracted in the dull regions to different extents in the two cases. A comparison of the particle size distributions and aspect ratio distributions in different regions established that rapid retraction of the suspended elastomer phase was the dominant cause of changes in particle shape between surface regions. Nonlinear shear creep and creep recovery curves of the two elastomer components showed that at a time of 1 s, the fractional strain recovery of the elastomer in B1 was much higher than that of the elastomer in B2. Hence, the nonlinear elastic recovery of the elastomer phase at short times is an important factor in flow mark formation with blends of polypropylene and olefinic elastomers. © 2005 Wiley Periodicals, Inc. J Appl Polym Sci 96: 423–434, 2005

Key words: blends; polyolefins; injection molding; morphology; rheology

INTRODUCTION

Surface defects known as tiger stripes have been observed on injection molded parts with a variety of thermoplastic materials, including neat polymers,[1–3] filled polymers,[4,5] and polymer blends.[5–11] Tiger stripes are alternating glossy and dull bands that form perpendicular to the flow direction. In many cases, the bands are asynchronous or out of phase on opposite surfaces of the part, with a glossy region on one surface of the part located across from a dull region on the opposite surface. Asynchronous flow marks differ from other defects in that as the injection speed is raised, they appear at shorter flow lengths, while higher melt and mold temperatures delay the onset.[4–6] The dull region is termed the flow mark, while the glossy region is termed the "out-of-flow mark." The contrast between these regions is an indication of the severity of the flow mark. The present article reports on an investigation of the microstructural differences between these regions and the material characteristics associated with both the onset and the severity of flow marks in high-speed injection molding of thermoplastic olefin (TPO) blends. These blends are dispersions of a random ethylene–propylene copolymer (EP) elastomer in a polypropylene (PP) matrix, providing toughened materials for various automotive parts including bumpers, where a uniform glossy surface finish is required.

Visual observations reported by several researchers[1,3,7,8] have demonstrated that flow marks are caused by a flow transition at the advancing melt front from stable symmetric fountain flow to unstable, oscillating, asymmetric flow. This nonideal, perturbed melt flow in the mold cavity is characterized by a shift of the stagnation point from the mid plane of the channel towards one of the mold walls, as shown in Figure 1. This also leads to flow paths of different lengths from the stagnation point to the opposing walls, with the melt experiencing different strain histories on the two flow paths. This could have more noticeable effects on filled systems. Indeed, Mizutani et al.[4] and Hobbs[5] reported that larger filler particles

Correspondence to: K. Jayaraman (jayarama@egr.msu.edu).

Journal of Applied Polymer Science, Vol. 96, 423–434 (2005)

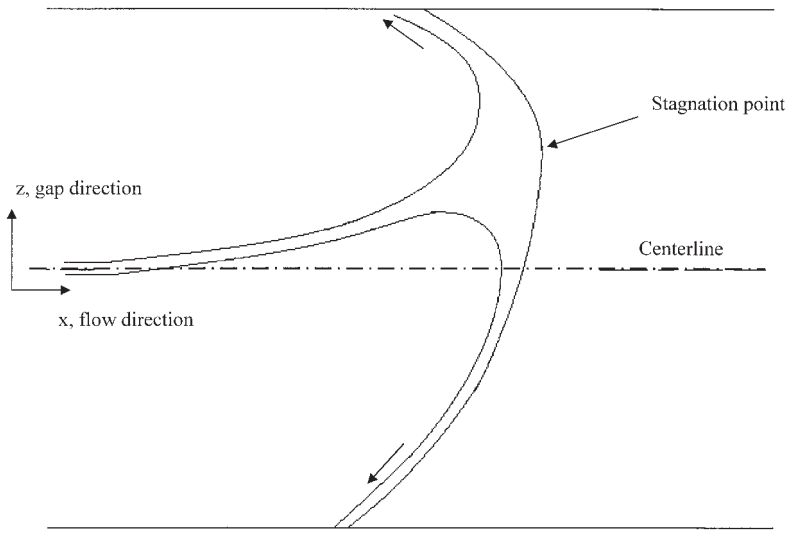

Figure 1 An unstable, advancing melt front during injection molding with flow marks, showing asymmetric path lines and an offset stagnation point.

and higher concentrations of the filler enhanced the contrast between the flow-mark and out-of-flow-mark regions. Hamada and Tsunasawa[7] studied the morphology of injection-molded tensile bars made with blends of polycarbonate (PC) and acrylonitrile-butadiene-styrene (ABS) and reported a similar flow transition with the flow of these PC/ABS blends, too. With the help of chromic acid etching to remove ABS particles at the surface and scanning electron microscopy, they reported different phase concentrations at the surface in different regions with these blends: the glossy out-of-flow-mark region was polycarbonate rich at the surface, while the flow-mark region displayed both components at the surface. Edwards and Choudhary[11] have also examined variations in surface morphology of injection molded plaques from a PC/ASA (acrylonitrile-styrene-acrylate) blend and confirmed the presence of a polycarbonate rich skin in glossy regions; they attributed this in part to a lower surface energy for the PC phase. However, they observed a different type of defect that improves with increasing injection rates.

The effect of melt rheology on this phenomenon has been studied experimentally with neat melts and rigid particle filled melts by Mizutani et al.[4] In studies with single phase polypropylene melts, they reported that higher melt viscosity and higher number average molecular weight led to more severe flow marks. In studies with filled polymers, Mizutani et al.[4] reported that the matrix with high polydispersity led to delayed onset of the instability and to lower contrast between glossy and dull surfaces. This effect of increasing matrix polydispersity or matrix viscoelasticity was confirmed even with polymer blends by Chang,[6] who ignored the characteristics of the dispersed phase. It is worth noting here that recent numerical analysis of single-phase flow stability near the advancing melt front by Bogaerds et al.[12] predicts that the onset of flow marks is delayed in melts that display greater strain hardening in extensional flow. Hence, there is a need to characterize the molten polymer blend and the components in extensional flow and understand the effects of the blend rheology and the dispersed elastomer rheology on the phenomenon of asynchronous flow marks.

The objectives of this study were to investigate with thermoplastic olefin blends: (1) the disperse phase morphology in flow-mark regions relative to that in out-of-flow-mark regions, and (2) the effects of the blend rheology and of the elastomer rheology on the severity of flow marks in two different TPO blends. It will be demonstrated in this article that the disparities in dispersed phase microstructure between the flow-mark and out-of-flow-mark regions are greater when the elastomer phase displays a greater extent of recovery on the time scale of injection molding.

EXPERIMENTAL

Materials

Two reactor-made TPO blends labeled B1 and B2 were studied. The matrix phase in B1 is a copolymer of polypropylene with 3 wt % ethylene, while the matrix in B2 is a PP homopolymer. The dispersed elastomer phase in B1 is a random ethylene–propylene copolymer with 35 wt % propylene, while the dispersed elastomer phase in B2 is a random ethylene–propylene copolymer with 45 wt % propylene. The composition of these blends and the component properties are summarized in Table I. The components of the reactor-made blends were separated by solvent extraction of

TABLE I
Composition of the Reactor-Made Blends and Component Properties at 200°C

Blend	B1	B2
Matrix specifications		
Composition	Polypropylene copolymer with 3 wt % ethylene	Polypropylene homopolymer
MFR [dg/min]	31	25
η_0 [Pa-s]	920	1010
$\lambda_0 = \eta_0 J_e^0$ [s]	48	7
Dispersed phase specifications		
Composition	Ethylene–propylene random copolymer (EP)	Ethylene–propylene random copolymer (EP)
MFR	6.4	8.0
Ethylene/propylene wt. ratio	65/35	55/45
η_0 [Pa-s]	69400	15750
J_e^0 [Pa^{-1}]	0.39×10^{-2}	1.15×10^{-2}
λ_0 [s]	273	181
Wt % EP in blend	32	35

the polypropylene matrix with boiling xylene as the solvent. The EP phase has a small xylene soluble fraction that is extracted with the PP in this process.

Injection molding

A standard tensile bar mold cavity (16 cm × 1.8 cm × 0.3 cm) was used with a mold wall temperature of 24°C, a melt injection temperature of 202°C, and an 8 s fill time. In addition to making full tensile bars for comparing the extent of tiger striping with the two blends, short shots of roughly half the mold volume were also made, with an injection time of 4 s. Stroke lengths of 1.32 cm and 1.35 cm, respectively, were used with blends B1 and B2 (a stroke length of 2.3 cm corresponds to a full shot). Short shots allow us to evaluate the two-phase morphology near the advancing melt front and interpret the dispersed phase deformation observed in the flow-mark and out-of-flow-mark surfaces.

Morphological characterization

Scanning electron microscopy (SEM) specimens were prepared by etching with methyl-cyclohexane to dissolve the EP elastomer phase, which leaves voids that appear dark in the micrographs. Sections were microtomed from the two different surface regions (x-y plane), two near wall regions (x-z plane), and the core region near the flow front (x-z plane) of the short shot, as shown in Figure 2. The SEM images were analyzed with the help of image analysis software packages from Sigma Scan (Jandel Scientific, Sigma Scan Pro 3.0) and Scion Image (Scion Corp., Scion Image Version 3b).

Rheological characterization

Test specimens for rheological characterizations were made by compression molding powder or pellets into disks with a 10 ton force over 5 min at 200°C. The blends and the component materials were subjected to

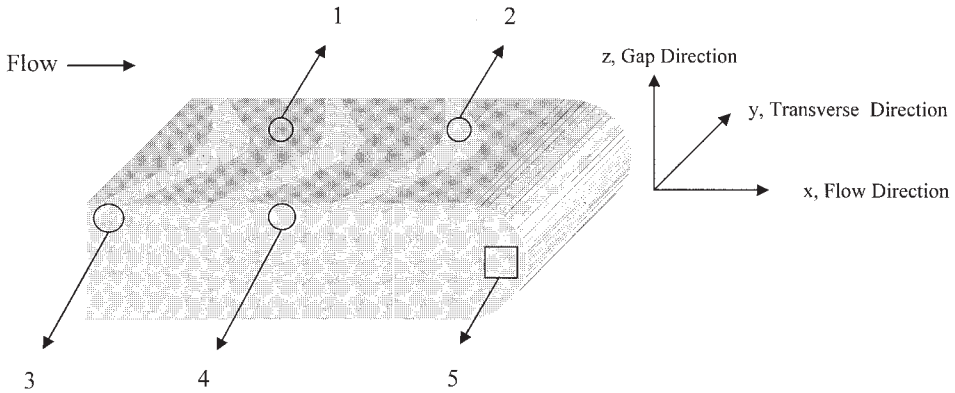

Figure 2 Various regions marked on a short shot for SEM image analysis: (1) Out-of-flow-mark (glossy) surface, x-y plane; (2) Flow-mark (dull) surface, x-y plane; (3) Near-wall cross section beneath flow-mark region, x-z plane; (4) Near-wall cross section beneath out-of-flow-mark region, x-z plane; (5) Cross section of core upstream of flow front, x-z plane.

oscillatory shear on a Rheometrics Mechanical Spectrometer RMS-800 at 200°C using a 50 mm parallel plate configuration. Frequencies ranging from 0.02–200 rad/s were employed. A strain sweep was conducted at several frequencies to identify the maximum strain for testing in the linear viscoelastic range. The blends were also characterized in steady shear at shear rates ranging from 0.1–200 s^{-1}. The linear viscoelastic transient viscosity growth η_0^+ was measured for these materials at a shear rate of 0.005 s^{-1} in a TA Instruments AR 2000 rheometer with 25 mm parallel plates.

Shear creep and recovery curves were recorded by operating the TA Instruments AR 2000 rheometer in the controlled stress mode with 25 mm parallel plates. The zero-shear viscosity η_0 and the characteristic relaxation time λ_0 of the blend components at 200°C were obtained from linear shear creep measurements at low stresses (ranging from 5–50 Pa). Other nonlinear viscoelastic tests were conducted at 180°C, where creep was recorded up to a strain of 10 at shear stresses ranging from 100 to 3000 Pa; these curves were shifted by time–temperature superposition to 200°C. The lower temperature was used to minimize degradation at the long times involved. Upon attainment of the desired strain, γ_{max} (at time $t = t_1$), the stress was set to 0 and the strain recovery was recorded at subsequent times ($t' = t - t_1$.) The instantaneous strain during recovery $\gamma(t')$ is subtracted from γ_{max} to obtain the recoverable strain $\gamma_r(t')$.

$$\gamma_r(t') = \gamma_{max} - \gamma(t') \tag{1}$$

Extensional viscosity

The melt extensional viscosity (η_E) was measured with lubricated skin-core flow through a semihyperboloidal die[13–15] fitted in a Dynisco capillary rheometer. The die profile is given by $r^2(z + z_0) = constant$, as shown in Figure 3. The die chosen here offers a fixed Hencky strain of 4.9 based on the entrance and exit cross-sectional areas as defined below.

$$\varepsilon_H = \ln\left(\frac{A_{entrance}}{A_{exit}}\right) \tag{2}$$

The inlet diameter of the die is the same as that of the rheometer barrel. The die profile is designed to provide a uniform extensional strain rate ($\dot{\varepsilon}$), for a given piston velocity (V_p).

$$\dot{\varepsilon} = \frac{V_P}{L}\exp\varepsilon_H \tag{3}$$

where L is the length of the die. The flow of the test polymer was lubricated with an immiscible, low-viscosity LLDPE "skin" (made from Dowlex LLDPE 2503, MFR = 105). Prefabricated skin-core billets, with core/skin ratio of 70/30 by volume to ensure proper lubrication, were used for measurements. With adequate lubrication, the pressure drop ΔP over the die length can be used to evaluate a "strain averaged" extensional viscosity η_E as follows[14,15]:

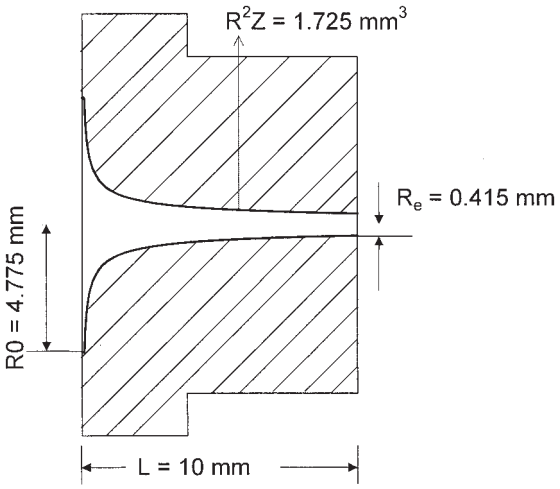

Figure 3 Profile of the semihyperboloidal converging die, designed to provide uniform extensional strain rates and a Hencky strain of 4.9.

$$\eta_E(\dot{\varepsilon},\varepsilon_H) = \Delta P/\dot{\varepsilon}\varepsilon_H \tag{4}$$

Extensional viscosities of the blend components were thus measured at strain rates ranging from 0.5–25 s^{-1}. The pressure transient in each run was carefully monitored for stable flow before recording the pressure drop. A strain hardening parameter (χ) in extension was evaluated with respect to three times the linear viscoelastic startup shear viscosity growth function as shown below[16]:

$$\chi(\varepsilon_H,\dot{\varepsilon}) = \eta_E^+(\dot{\varepsilon},\varepsilon_H)/3\eta_0^+(t = \varepsilon_H/\dot{\varepsilon}) \tag{5}$$

The linear viscoelastic shear viscosity transient in the denominator was evaluated at a time equal to the residence time of the melt in the semihyperboloidal die for a chosen strain rate.

RESULTS AND DISCUSSION

Flow-mark frequency and blend rheology

Flow marks are observed in tensile bars molded from both blends; the difference between the flow-mark patterns obtained with blends B1 and B2 is illustrated in Figure 4. The flow marks are spaced closer together in the bars from B1; the flow-mark spacing (distance between the centers of two neighboring flow marks) is 15 mm in the B1 tensile bars and 20 mm in the B2

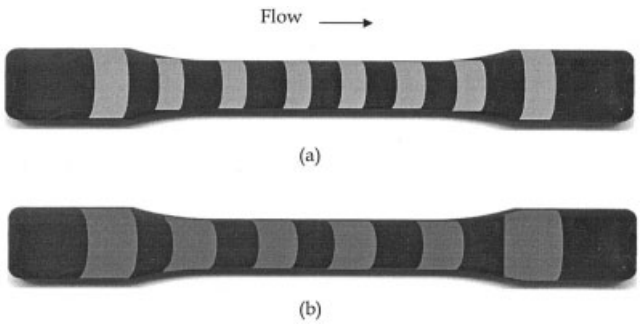

Figure 4 Comparison of flow marks on tensile bars of two different blends: (a) Blend B1 with a high surface contrast between glossy (out-of-flow-mark) and dull (flow-mark) regions; (b) Blend B2 with a lower surface contrast.

tensile bars. It is clear from the greater number of flow marks on bars molded from B1 that the instability is more pronounced in blend B1. The flow front must oscillate with greater frequency during injection molding of blend B1 to produce the observed surface patterns. It is worth noting here that the melt injection rate was not varied in this work.

Of several rheological tests conducted on the two blends—steady shear viscosity curves, nonlinear extensional viscosity in flow through a semihyperboloidal die, linear viscoelastic shear creep recovery, and linear transient viscosity growth—the latter two tests showed the most difference between the two. The two blends have very similar steady shear viscosity curves as shown in Figure 5. The linear shear creep recovery curves plotted in Figure 6 show clearly that the recovery is faster in B1 than in B2. The linear viscoelastic limit of extensional viscosity growth is 3 times the linear viscoelastic shear viscosity growth obtained at very low strain rates and is plotted in Figure 7 for the two blends. These curves are noticeably different for the two blends, with B1 having the faster response.

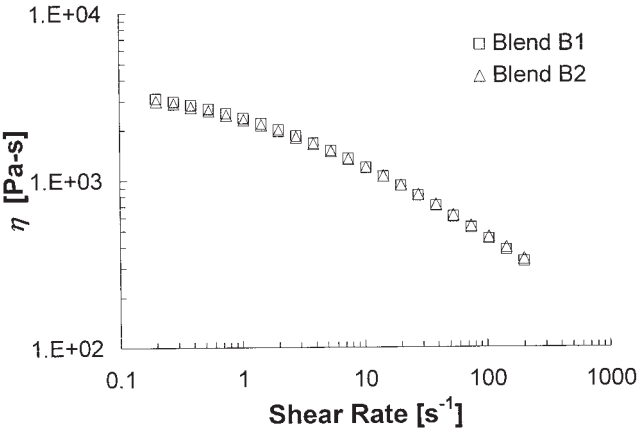

Figure 5 Shear viscosity curves of the reactor-made blends B1 and B2 measured at 200°C.

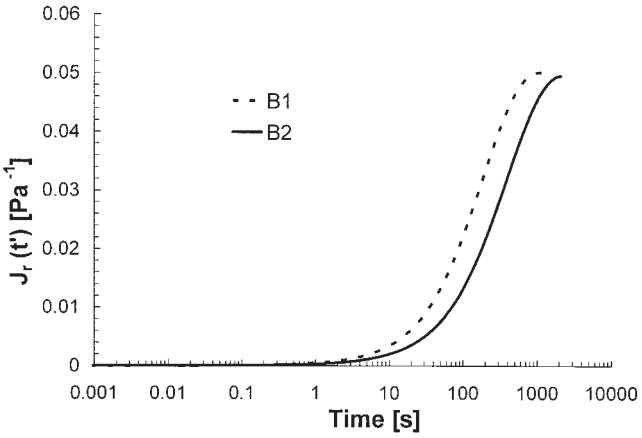

Figure 6 Linear shear creep recovery curves for the two blends at 200°C.

The nonlinear strain averaged extensional viscosity η_E^+ at a total Hencky strain of 4.9 is also plotted in Figure 7 as a function of the residence time $t = 4.9/\dot{\varepsilon}$ for several strain rates. Relative to the magnitude of $3\eta_0^+(t)$ at comparable times ($t = 4.9/\dot{\varepsilon}$), the nonlinear extensional viscosities of both blends are higher at all the strain rates. Thus, both blends exhibit extensional strain hardening. Although the extensional viscosity curves are close for the two blends, the strain hardening relative to the linear viscosity growth is lower in B1, especially at high strain rates, as shown in Figure 8. From Figure 8, it is also clear that the strain hardening parameter (χ, cf. eq. (5)) shows a steeper decline with increasing strain rate for blend B1 than for blend B2. The higher frequency of flow marks in blend B1 goes with the lower extent of strain hardening in this blend. Hence, trends in the degree of strain

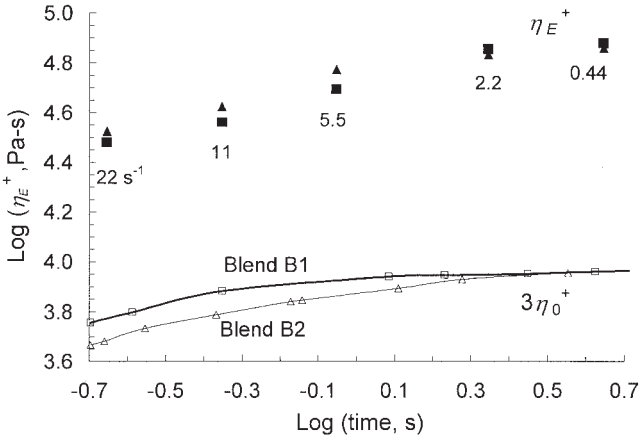

Figure 7 Three times the linear shear viscosity growth as a function of time at a low strain rate (0.005 s^{-1}) for the two blends; and nonlinear strain averaged extensional viscosity of blends B1 (■) and B2 (▲) evaluated at Hencky strain $\varepsilon_H = 4.9$ and 200°C, plotted as a function of the residence time in the semihyperboloidal die.

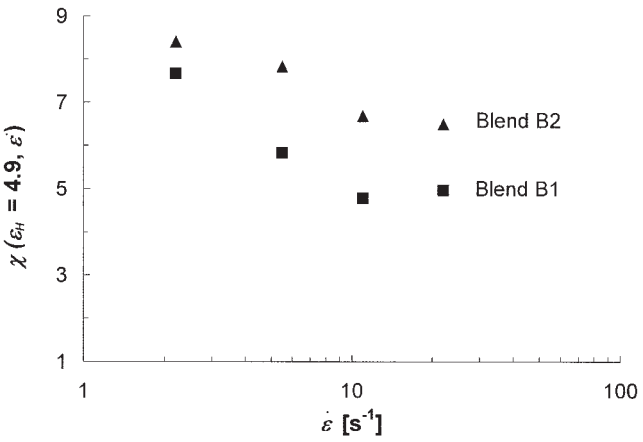

Figure 8 Extensional strain hardening parameter χ for the TPO blends evaluated at a Hencky strain $\varepsilon_H = 4.9$ and 200°C.

hardening of the blends and the frequency of flow marks appear to be consistent with the predictions of Bogaerds et al.[12]

Surface morphology of injection-molded short shots

The contrast or difference in gloss between the out-of-flow-mark and flow-mark regions is also more striking in the bars molded from B1 than in the bars from B2. Representative SEM micrographs of these regions and of the core near the flow front in short shots are presented in Figures 9–11 for blend B1 and in Figures 12–14 for blend B2. Two orthogonal views were obtained for the flow-mark and out-of-flow-mark regions; the core region of the flow front was viewed only in the x-z plane. The surface morphology in the x-y plane is presented in a zoom view as well in Figures 10 and 13. These figures show that for the TPO blends of this study, the disperse phase is present in both regions, in contrast to observations of Hamada and Tsunasawa[7] with PC/ABS blends. The following analysis will also show that the particle concentration is the same in these regions. The near wall micrographs in the x-z plane (Figs. 11 and 14) reveal that the surface morphology extends to a depth of 20–30 μm. It is apparent from combining the surface micrographs with the near-wall micrographs that in the case of B1, the elastomer particles in the out-of-flow-mark region are cylindrical with axes oriented along the flow direction, while the particles in the flow-mark region are elliptical disks with the disk thickness aligned with the z-coordinate along the mold gap. In the case of B2, the elastomer particles are uniformly cylindrical in the out-of-flow-mark region but in the flow-mark region, the strands are shorter and thicker on one end. In both blends, the particles are much more stretched and oriented in the out-of-flow-mark regions than in the flow-mark regions; the difference in particle shapes between regions is very prominent in the case of B1.

The change of particle shape between the surface regions could be caused by a combination of retraction, breakup, and coalescence of the dispersed phase. To identify the dominant mechanism among these, a quantitative comparison of particle sizes and aspect ratios in the two types of surface regions was carried

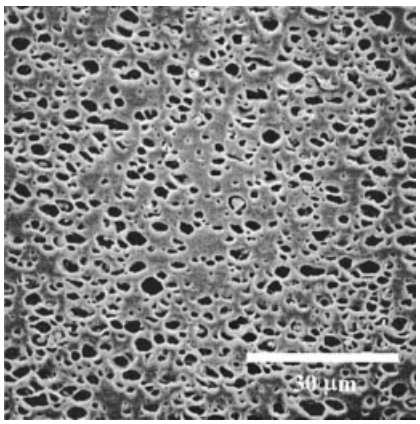

Figure 9 x-z plane section near the flow front in the core region of blend B1.

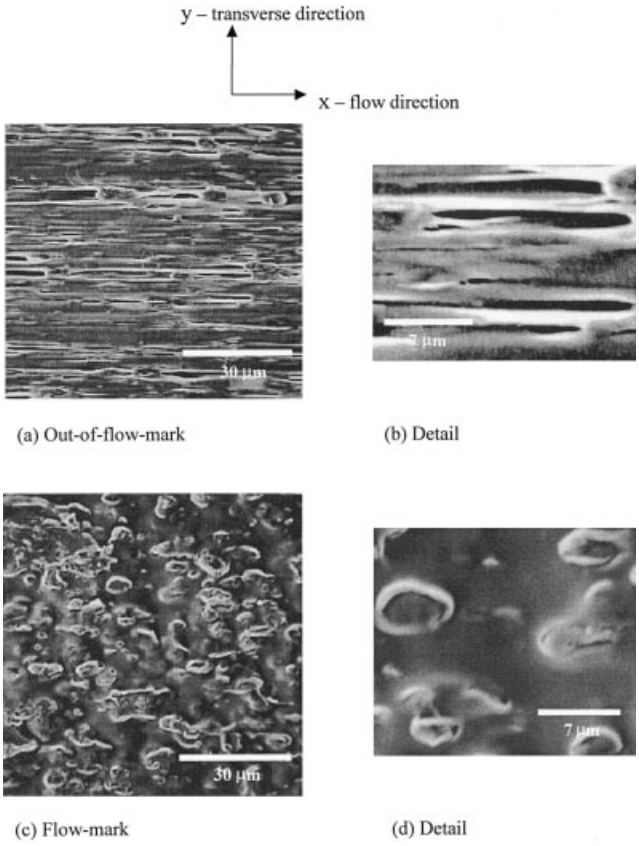

Figure 10 x-y plane sections from out-of-flow-mark and flow-mark surfaces in blend B1.

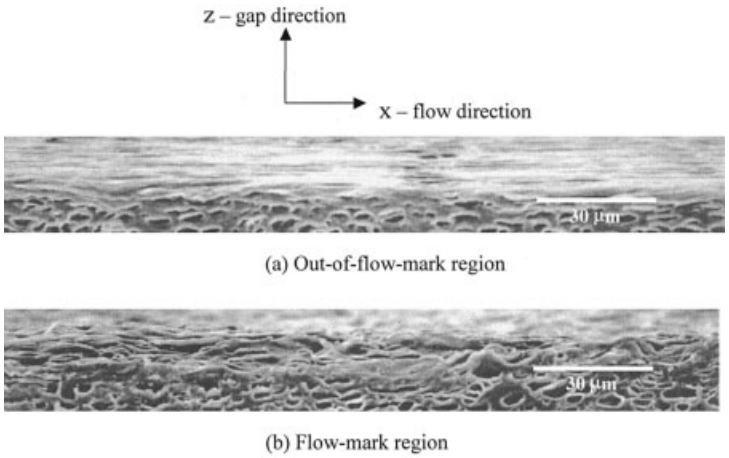

Figure 11 Near-wall sections in the x-z plane beneath the out-of-flow-mark and flow-mark surfaces of blend B1.

out with several micrographs for each case. The total micrograph area analyzed was the same for both out-of-flow-mark and flow-mark regions, and the results are listed in Table II. The particle size distributions in the various regions including the core are presented in Figure 15(a) for B1 and in Figure 15(b) for B2. In both cases, the particle sizes are more nearly uniform in the core region than in the surface regions; and the particle size distributions in both types of surface regions are broad and bimodal. For B1, the first peak of these distributions for smaller particles is at the same size for the two surface regions and also matches that for the core. The area under this peak is also the smallest for the flow-mark region. These trends indicate that there was no drop breakup in the transition between the two surface regions. For B2, the first peak for both surface regions is again at the same size, and this size is bigger than the corresponding size for the core; the area under the first peak is also smallest for the flow-mark region. These trends eliminate drop breakup as a cause of the change between the two surface regions.

The mean particle projected area in different regions is listed, along with mean dimensions, in Table II. It is worth noting that the mean x and y dimensions for the surface regions were based on a large number of particles, but the z-dimension was not; the number of particles in the near-wall x-z micrographs was much less than in the x-y surface micrographs. The mean particle area and the characteristic z-dimension have

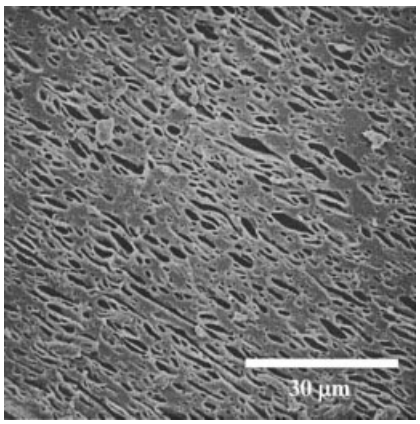

Figure 12 x-z plane section near the flow front in the core region of blend B2.

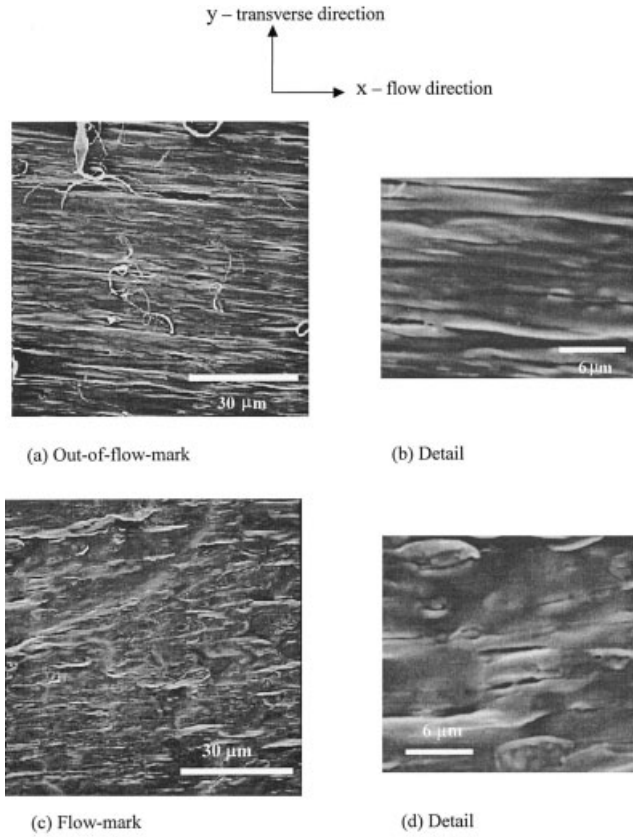

Figure 13 x-y plane sections from out-of-flow-mark and flow-mark surfaces in blend B2.

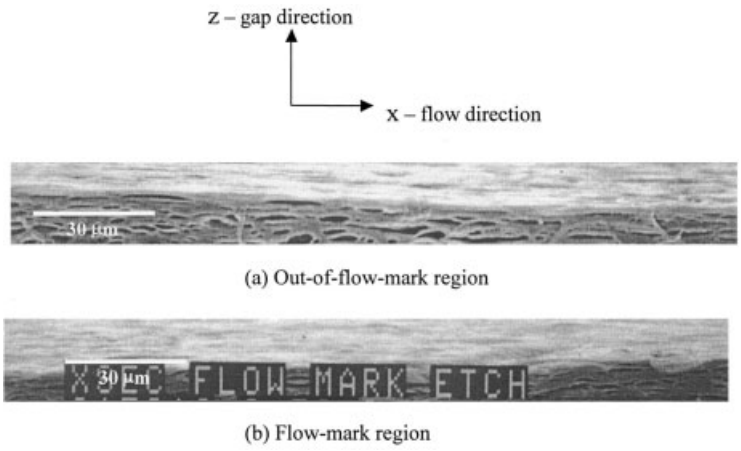

Figure 14 Near-wall sections in the x-z plane beneath the out-of-flow-mark and flow-mark surfaces of blend B2.

been put together to evaluate a representative particle volume for each region, with a specified shape; this is also tabulated in Table II. Comparison of the mean particle volume appears to indicate some coalescence, especially in the case of B1. The total particle volumes associated with different regions were very close, demonstrating that the volume fraction of particles was the same in both types of surface regions.

The differences in degree of stretch between the surface regions may be examined first by evaluating the particle aspect ratios in the x-y plane. The aspect ratio distributions for the dispersed phase in various regions are presented in Figure 16(a) for B1 and in Figure 16(b) for B2. The aspect ratio recorded in the x-y projection is a true aspect ratio because a high degree of particle alignment is observed in both orthogonal planes (x-y and x-z) for all particle projections near the wall. The aspect ratio distribution is very broad for the out-of-flow-mark region in both cases. Compared to the aspect ratio distribution for the core region, which is narrow with a mean of about 2 in both cases, this signifies a broad range of stretch for the particles in the out-of-flow-mark regions. The two blends are quite different in the aspect ratio distributions of the flow-mark regions. The aspect ratio distribution is quite narrow for the flow-mark region in the case of B1, with a mean of 2.1. Compared to the mean aspect ratio of 11.5 for particles in the out-of-flow-mark region in B1, this would indicate that the particles are retracting to a more isotropic shape. The aspect ratio distribution in the flow-mark region for B2 is broader than for B1 and has a mean of 8.1. Compared to the mean aspect ratio of 12.5 in the out-of-flow-mark region for B2, this would indicate incomplete retraction, as is evident from the images themselves. As noted earlier, the retraction is evident in the strands, with one of the ends becoming thicker. A further indication of the extent of retraction may be obtained by comparing stretch ratios for the two regions. A stretch ratio may be defined as $\bar{x}/2R_{eq}$, the ratio of the particle dimension along the flow (x-) direction to the diameter of the equivalent sphere

TABLE II
Results of Morphology Analysis on Injection Molded TPO Short Shots (see Fig. 2 for coordinate labels)

	Blend B1			Blend B2		
Property	Core	Out-of-flow-mark	Flow-mark	Core	Out-of-flow-mark	Flow-mark
Total micrograph area [μm^2]	8245	8229	8280	8244	8229	8280
# of particles in micrograph	1373	493	228	2068	433	350
Mean projected particle area [μm^2]	1.25	2.8	4.2	0.9	3.8	3.0
Mean x-dim [μm]	1.4	5.6	2.9	1.4	7.2	5.4
Mean y-dim μm]	*	0.6	1.5	*	0.6	0.7
Characteristic z-dim [μm]	0.8	0.6	0.7	0.5	0.6	0.9
Mean aspect ratio	1.8	11.5	2.1	2.6	12.5	8.2
Mean particle volume [μm^3]	*	1.3	2.9	*	1.7	2.0
Equivalent sphere radius $R_{eq.}$ [μm]	*	0.7	0.9	*	0.7	0.8
Stretch ratio = $x/(2R_{eq})$	*	4	1.6	*	5.1	3.4

* Only x-z plane micrographs were available for the core region.

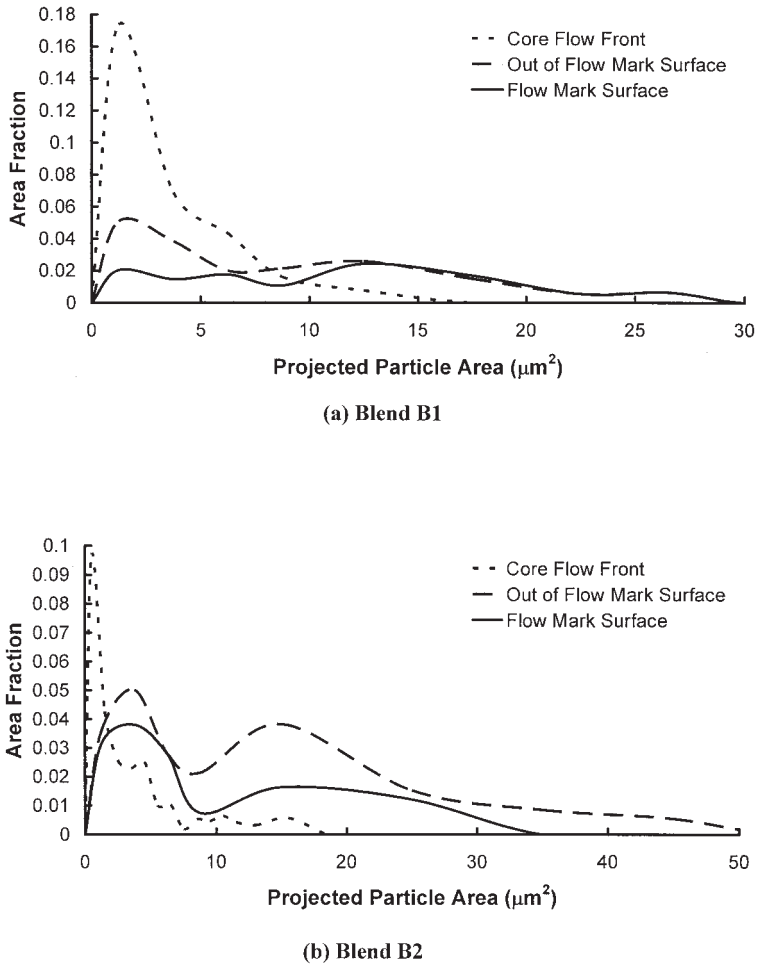

Figure 15 Projected area distributions of the dispersed elastomer particles in various regions of (a) B1 and (b) B2.

($2R_{eq}$). As seen in Table II, for B1, the stretch ratio declines from 4 for the out-of-flow-mark region to 1.6 for the flow-mark region. For B2, the stretch ratio declines from 5.1 for the out-of-flow-mark region to 3.4 for the flow-mark region. This establishes retraction of stretched elastomer particles as a dominant mechanism for the change of shape. Hence, the contrast between flow marks and other regions on the surface is governed by the extent of recovery from stretching of the elastomer phase.

Rapid retraction and elastomer rheology

It remains to relate the rheology of components in the blends to observed differences in the extent of recovery of the dispersed phase in the two blends. It is important to note that the timescales available during injection molding operations for the observed recovery are of the order of seconds. Over such times, the elastomer recovery must be driven by elastic stresses rather than interfacial tension. Interfacial tension driven recovery is much slower than injection rates and is usually completed over several thousand seconds, particularly under quiescent no-flow conditions as reported by Cohen and Carriere,[17–19] Rundqvist et al.,[20] and Gramespacher and Meissner.[21,22] The matrix viscosity and relaxation time will affect this rate as well.[23,24] The shear viscosity curves presented in Figure 17, as well as the extensional viscosity curves presented in Figure 18, of the dispersed EP elastomers in B1 and B2 are much higher than the corresponding curves of the matrix polypropylenes (PP), which have very similar viscosity curves in both shear and extension. The characteristic relaxation times of the EP elastomers (see Table I) are also higher than those of the matrix polypropylenes so that flow induced stresses would decay faster in the matrix PP phase than in the dispersed EP phase. Hence, it is appropriate to examine the recovery of the elastomer phase in the two blends at short times. This was done with nonlinear shear creep and recovery tests.

The nonlinear creep curves $\gamma(t)$ have been recorded up to a shear strain of 10 at 200°C and stresses ranging from 100 Pa to 3000 Pa; the stress is then released and the creep recovery transients $\gamma_r(t')$ are recorded. These curves have been plotted together for the high-

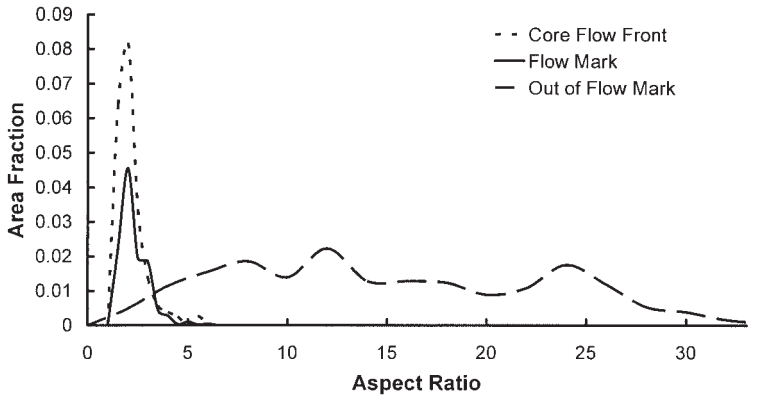

(a) Blend B1

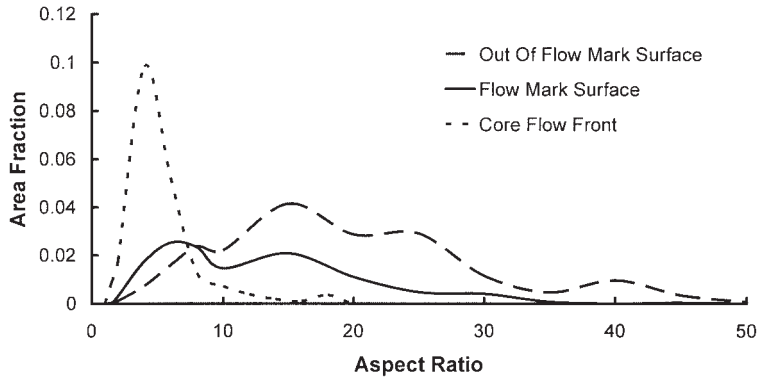

(b) Blend B2

Figure 16 Aspect ratio distributions of the dispersed elastomer particles in various regions of (a) B1 and (b) B2.

est tested shear stress $\tau = 3000$ Pa in Figures 19(a) and (b) for the dispersed EP elastomers in B1 and B2, respectively. As shown by Munstedt and coworkers,[25,26] each point γ_r (t') on the recovery curve also represents the recoverable strain in the elastomer melts when deformed to a total strain γ (t) that is less than the maximum strain of 10 under the imposed

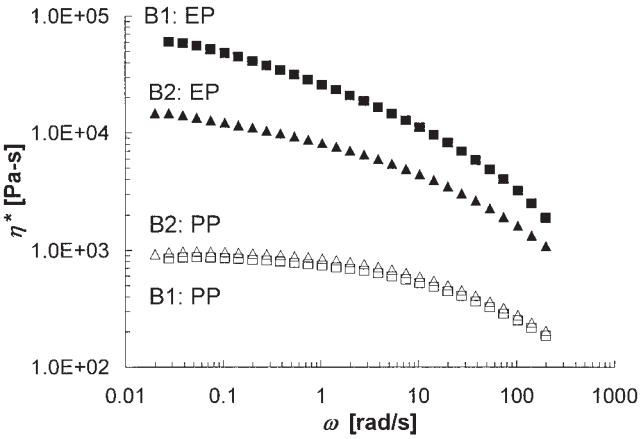

Figure 17 Dynamic shear viscosity curves of the PP matrices and EP dispersed phases of the blends at 200°C.

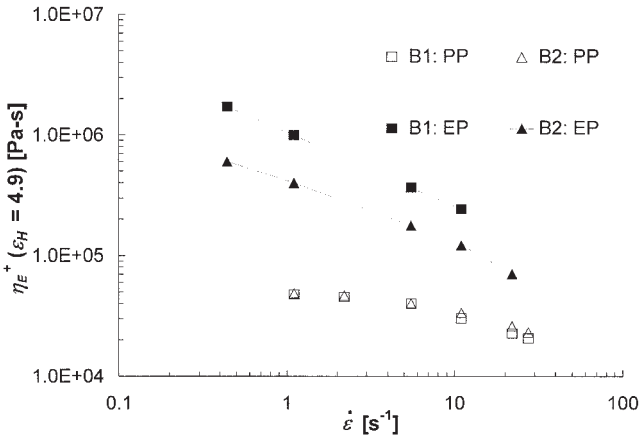

Figure 18 Strain averaged extensional viscosity of the matrix PP (open symbols) and dispersed EP elastomer phases (filled symbols) of blends B1 and B2, evaluated at a Hencky strain of 4.9 and at 200°C.

stress. Figure 19 shows that the transient recoverable strain is higher in the EP phase of B1 than in B2. The ratio of recovered strain relative to the imposed strain at times of 1 to 2 s is relevant because these are the timescales of interest in rapid processing operations, such as injection molding. At times of the order of 1–2 s, the recoverable strain for the elastomer in B1 closely follows the total strain, while the recoverable strain of the elastomer in B2 is significantly lower than the imposed strain.

The transient recoverable strain at 1 s from the nonlinear creep recovery experiments conducted at 200°C is plotted against the creep stress (τ) for the elastomers in B1 and B2 in Figure 20. In this figure, the recoverable strains at $t' = 1$s during recovery have been scaled by the linear equilibrium recoverable strain ($J_e^0\tau$) corresponding to that stress. This figure shows that the short time recovery of the elastomer in B1 is consistently higher over the entire range of stress. The trends in shear creep recovery are consistent with the extents of recovery observed in the dispersed EP phases in flow-mark regions of the injection molded

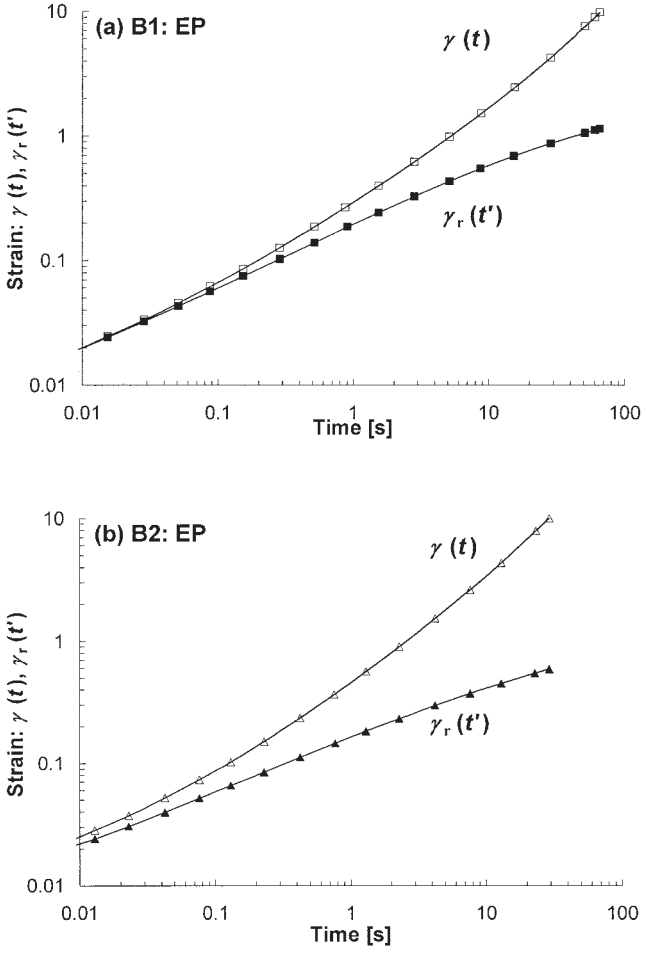

Figure 19 Total strain and recoverable strain during shear creep at 3000 Pa followed by constrained recovery for the EP elastomer phases of the blends at 200°C.

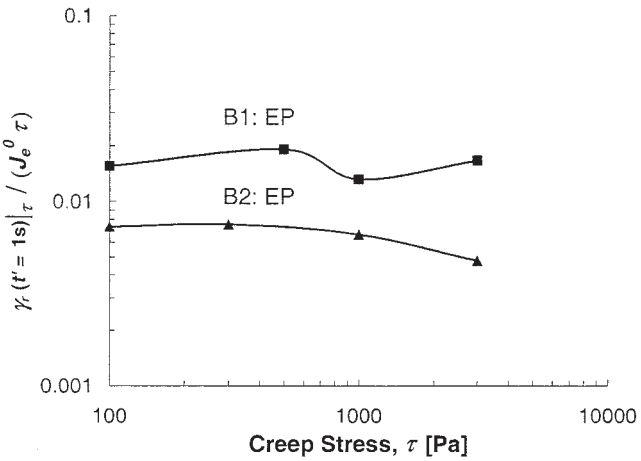

Figure 20 Recovered strain $\gamma_r(t' = 1\text{ s})$ relative to the linear equilibrium recoverable strain corresponding to the creep stress during constrained recovery following shear creep at several stresses for the EP elastomer phases of the two blends, and at 200°C.

articles. Similar trends are to be expected in recovery following extensional flow at the advancing flow front. Experiments for investigating rapid recovery of suspended elastomer drops following controlled extensional flow are underway in our laboratory.

CONCLUSIONS

Asynchronous flow marks on the surface of tensile bars injection molded from different reactor-made blends of polypropylene and ethylene–propylene copolymer elastomers in the same proportions have been found to appear with a greater frequency for the blend B1, which also exhibited a greater contrast between the surface regions. The linear shear creep recovery and the linear viscoelastic shear viscosity growth of B1 were faster than for B2. The major difference between surface regions was found to be in the degree of stretching and orientation of the dispersed elastomer phase. The dispersed phase was highly stretched to cylindrical strands with a mean aspect ratio of about 12 in the glossy surface regions of both blends, while it was retracted in the dull regions to different extents in the two cases. The retracted shape in the dull surface region was that of a disk for blend B1, and the contrast between the regions was most striking. In the other blend, B2, the partially retracted shape was that of shorter strands with a mean aspect ratio of 8 that were thicker at one end, and the contrast between the regions was less severe. A comparison of the particle size distributions in different regions established that rapid retraction of the suspended elastomer phase was the dominant cause of changes in particle shape between surface regions. The two matrix polymers in B1 and B2 had very similar shear viscosity curves as well as extensional viscosity curves, but the elastomers in the two

blends showed large differences in these curves. Testing of the two elastomer components in nonlinear shear creep and creep recovery showed that at a time of 1 s, the fractional strain recovery of the elastomer in B1 was much higher than that of the elastomer in B2. Hence, the nonlinear elastic recovery of the elastomer phase at short times is an important factor in flow-mark formation with blends of polypropylene and olefinic elastomers.

This work was supported in part by Basell USA Inc. and by a scholarship awarded to Bhaskar Patham by the Detroit Section of the Society of Plastics Engineers for work on thermoplastic olefin blends. We are also pleased to acknowledge the assistance of Dr. Dinshong Dong of Basell Polyolefins in separating the components of the reactor-made blends.

References

1. Yokoi, H.; Nagami, S.; Kawasaki, A.; Murata, Y. SPE ANTEC Tech Papers (Society of Plastics Engineers, Brookfield, CT) 1994, 40, 829.
2. Heuzey, M. C.; Dealy, J. M.; Gao, D. M.; Garcia-Rejon, A. Intern Polymer Processing 1997, XII, 403.
3. Monasse, B.; Mathieu, L. PPS 15th Annual Conference (Polymer Processing Society, Akron, OH) 1999, Abstracts.
4. Mizutani, H.; Koizumi, J.; Ito, K.; Mukai, H.; Kawashima, D. SAE Tech. Papers (Society of Automotive Engineers, Warrendale, PA) 2000, Paper No. 2001–01-1127.
5. Hobbs, S. Y. Polym Eng Sci 1996, 32, 1489.
6. Chang, M. C. O. Intern Polymer Processing 1996, XI, 76.
7. Hamada, H.; Tsunasawa, H. J Appl Polym Sci 1996, 60, 353.
8. Grillet, A. M.; Bogaerds, A. C. B.; Peters, G. W. M.; Baaijens, F. P. T.; Butlers, M. J Rheol 2002, 46, 651.
9. Jayaraman, K.; Papworth, P.; Shu, C.; Wolkowicz, M. D. SPE ANTEC Tech Papers (Society of Plastics Engineers, Brookfield, CT) 2002.
10. Papworth, P. Master of Science Thesis, Michigan State University, East Lansing, MI, 2001.
11. Edwards, S. A.; Choudhary, N. R. Polym Eng Sci 2004, 44, 96.
12. Bogaerds, A. C. B.; Hulsen, M.A.; Peters, G. W. M.; Baiijens, F. P. T. J Rheol 2004, 48, 765.
13. Cogswell, F. N. J Non-Newton Fluid Mech 1978, 4, 23.
14. Everage Jr., A. E.; Ballman, R. L. Nature 1978, 273, 213.
15. Pendse, A. V.; Collier, J. R. J Appl Polym Sci 1996, 59, 1305.
16. Kurzbeck, S.; Oster, F.; Munstedt, H.; Nguyen, T. Q.; Gensler, R. J Rheol 1999, 43, 359.
17. Carriere, C. J.; Cohen, A.; Arends, C. B. J Rheol 1989, 33, 681.
18. Carriere, C. J.; Silvis, H. C. J Appl Polym Sci 1997, 66, 1175.
19. Cohen, C.; Carriere, C. J. Rheol Acta 1989, 28, 223.
20. Rundqvist, T.; Cohen, A.; Klason, C. Rheol Acta 1996, 35, 458.
21. Gramespacher, H.; Meissner, J. J Rheol 1997, 41, 27.
22. Gramespacher, H.; Meissner, J. J Rheol 1995, 39, 151.
23. Hooper, R. W.; de Almeida, V. F.; Macosko, C. W.; Derby, J. J. J Non-Newton Fluid Mech 2001, 98, 141.
24. Tretheway, D. C.; Leal, L. G. J. Non-Newton Fluid Mech 2001, 99, 81.
25. Gabriel, C.; Kaschta, J; Munstedt, H. Rheol Acta 1998, 37, 7.
26. Munstedt, H.; Laun, H. M. Rheol Acta 1979, 18, 492.